DEUTSCHES ELEKTRONEN-SYNCHROTRON DESY

DESY 84-101
October 1984

AN INVESTIGATION OF THE PROCESS $e^+e^- \to \mu^+\mu^-\gamma$

by

CELLO Collaboration

ISSN 0418-9833

NOTKESTRASSE 85 · 2 HAMBURG 52

To be sure that your preprints are promptly included in the
HIGH ENERGY PHYSICS INDEX ,
send them to the following address (if possible by air mail) :

DESY
Bibliothek
Notkestrasse 85
2 Hamburg 52
Germany

DESY 84-101
October 1984

An Investigation of the Process $e^+e^- \to \mu^+\mu^-\gamma$

CELLO Collaboration

Abstract

The reaction $e^+e^- \to \mu^+\mu^-\gamma$ has been studied with the CELLO detector at the PETRA storage ring. Data have been collected from $\sqrt{s}$ = 14 GeV up to 46.8 GeV. In a Dalitz plot analysis of the data, good agreement is found with QED for $\sqrt{s}$ = 14 and 22 GeV, while an excess of events is observed for $\sqrt{s}$ > 33 GeV and for $\mu\gamma$ masses above 30 GeV. The excess could be due to a statistical fluctuation, however with a probability at the 10^{-3} level.

An Investigation of the Process
$e^+e^- \to \mu^+\mu^-\gamma$

CELLO Collaboration

H.-J. Behrend, J. Bürger, L. Criegee, H. Fenner, G. Franke, J. Meyer, V. Schröder, H. Sindt, U. Timm, G.G. Winter, W. Zimmermann
Deutsches Elektronen-Synchrotron, DESY, Hamburg, Germany

P.J. Bussey, A.J. Campbell, J.B. Dainton, D. Hendry, G. McCurrach, J.M. Scarr, I.O. Skillicorn, K.M. Smith
University of Glasgow, United Kingdom

K. Paasch, M. Poppe, H. Spitzer
II. Institut für Experimentalphysik, Universität Hamburg, Germany

W.-D. Apel, J. Engler, G. Flügge, B. Forstbauer, D.C. Fries, W. Fues, K. Gamerdinger, P. Grosse-Wiesmann, Th. Henkes, G. Hopp, H. Jung, J. Knapp, M. Krüger, H. Küster, H. Müller, K.H. Ranitzsch, H. Schneider
Kernforschungszentrum Karlsruhe and Universität Karlsruhe, Germany

W. de Boer, G. Buschhorn, W. Christiansen, B. Fatah, G. Grindhammer, B. Gunderson, C. Kiesling, R. Kotthaus, H. Kroha, D. Lüers, H. Oberlack, P. Schacht, W. Wiedemann
Max-Planck-Institut für Physik und Astrophysik, München, Germany

G. Bonneaud[1], A. Cordier, M. Davier, D. Fournier, M. Gaillard, J.F. Grivaz, J. Haissinski, V. Journé, F. Le Diberder, U. Mallik[2], E. Ros, J.-J. Veillet
Laboratoire de l'Accélérateur Linéaire, Orsay, France

J.H. Field[3], R. George, M. Goldberg, O. Hamon, F. Kapusta, F. Kovacs, R. Pain, L. Poggioli, M. Rivoal
Laboratoire de Physique Nucléaire et Hautes Energies, Université de Paris, France

G. D'Agostini, M. Gaspero, B. Stella
University of Rome, and INFN, Italy

R. Aleksan, J. Bouchez, G. Cozzika, Y. Ducros, A. Gaidot, P. Jarry, Y. Lavagne, F. Ould Saada, J. Pamela, J.P. Pansart, F. Pierre
Centre d'Etudes Nucléaires, Saclay, France

G. Alexander, G. Bella, Y. Gnat, J. Grunhaus
Tel Aviv University, Israel

- to be submitted to Physics Letters B -

1) CRN Strasbourg, France
2) Now at SLAC, Stanford University, USA
3) On leave of absence from DESY, Hamburg, Germany

In this letter, we report on a study of the reaction

$$e^+e^- \to \mu^+\mu^-\gamma \qquad (1)$$

The data were obtained using the CELLO detector operating at the PETRA storage ring at DESY. This reaction should be well described by α^3 QED calculations[1]. Data have been collected over a wide energy range, from $\sqrt{s}$ = 14 GeV to 46.8 GeV, the maximum centre of mass energy reached by PETRA. While the data agree with QED below $\sqrt{s}$ = 33 GeV, an excess of events is observed at higher energies for $\mu\gamma$ masses above 30 GeV.

Detector Properties and Event Selection

The CELLO detector has been described previously[2]. The main feature of the CELLO detector used in this analysis is its good resolution and its large and uniform detection coverage for charged particles and photons. Charged particles are detected and analyzed in the angular range $30 < \theta < 150^0$ with a momentum resolution $\sigma_p/p^2 = 2\cdot10^{-2}$ (p in GeV/c) and angular resolutions $\sigma_\theta = 3 \text{ mr} \cdot \sin^2\theta$ and $\sigma_\phi = 2$ mr. Below $\theta = 30^0$, coverage is achieved down to 11^0 with increasingly worse resolution. Electromagnetic calorimetry is realized with a lead-liquid argon system in which granularity has been optimized both transversely and longitudinally, enabling a good angular resolution and a satisfactory hadron-muon/electron separation to be achieved. The photon angular resolutions are: $\sigma_\theta = (10 \pm 2)$ mr and $\sigma_\phi = (6 \pm 1)$ mr. The photon energy resolution is $\sigma_E/E = 5\% + 10\%/\sqrt{E}$ with E in GeV. The calorimeter covers 96% of the solid angle. Muons can be separated from electrons and hadrons by their characteristic minimum-ionizing behaviour in the calorimeter and their penetration through 80 cm of iron followed by their detection in wire chambers covering 92% of the solid angle. The minimum momentum for μ detection in the muon chambers is 1.4 GeV/c. The detector is triggered by combinations of charged tracks and electromagnetic energy. Reaction (1) was recorded by two independent triggers: one using two charged tracks, the other requiring a single track and an energy deposition in liquid argon greater than 2 GeV. It was therefore possible to crosscheck the triggers involved for reaction (1) and achieve an overall trigger efficiency of $\sim$95% within the detection solid angle described below.

The candidates for reaction (1) have been selected with the following criteria:

(i) only two tracks with $|\cos\theta| < .85$ with a momentum larger than .05 E_{beam}. In addition, the acoplanarity angle was required to be between 2^0 and 178^0.

(ii) One photonic shower with $|\cos\theta| < .85$ and energy larger than .10 E_{beam}; no other significant shower in the calorimeter was allowed (> .5 GeV).

(iii) a minimum angle of 10^0 between the photon and muon directions to avoid colinear radiation and confusion with $\tau\tau$ events where a $\pi\pi^0$ final state could simulate the $\mu\gamma$ topology.

(iv) a minimum visible energy of .6 $\sqrt{s}$ to eliminate remaining $\tau\tau\gamma$ events.

(v) a minimum value of .05 $\sqrt{s}$ for the $\mu\mu$ mass in order to avoid the contamination of $\gamma\rho^0$ events.

Muons were identified by dE/dx in the calorimeter or a recorded hit in the chambers surrounding the iron absorber: the distribution of energy deposited in the calorimeter for the final sample is given in Fig. 1a and the ratio of the distance between the extrapolated impact of the track in the muon chamber and the recorded hit to the estimated position uncertainty is shown in Fig. 1b. In addition, all the candidates were visually scanned before applying the identification cuts to avoid any systematic effects. The similar reaction

$$e^+e^- \to e^+e^-\gamma \qquad (2)$$

is also well identified and although its rate is typically one order of magnitude larger, its misidentification as reaction (1) is negligible (less than 10^{-3} of the $\mu\mu\gamma$ rate). The contributions from the reactions

$$e^+e^- \to \tau^+\tau^- \qquad (3)$$

and

$$e^+e^- \to \tau^+\tau^-\gamma \qquad (4)$$

are to a large extent removed by scanning since the final state involves π^0's and hadronic showers for most of the τ decays[3]. The

remaining part, which can simulate reaction (1), is considerably reduced by the kinematic constraints applied (discussed below), since missing neutrinos are always present in reactions (3) and (4).

The reaction

$$ee \rightarrow \pi^+\pi^-\gamma \qquad (5)$$

can be recognized by hadronic showers in the calorimeter. The non-observation of such events allows from the purely experimental point of view to set a limit of $6 \cdot 10^{-2}$ of the observed $\mu\mu\gamma$ rate to be due to reaction (5). An estimation which takes into account pion form factors gives a maximum possible contamination of $1\ 10^{-4}$.

Table I shows the data sample obtained at the different centre of mass energies.

Kinematic Reconstruction and Mass Resolution

The complete measurement of reaction (1) is kinematically overconstrained (4C). However angular measurements are more precise in our detector than energy measurements, at least for particles above $\sim$4 GeV. Therefore, the kinematics of reaction (1) can be precisely reconstructed from accurate angular determinations. Furthermore, it is possible to take into account the possible emission of a radiative photon along the incident electron or positron directions and to calculate the energies of the four final state particles.

Such a calculation has been performed on our event sample resulting in a distribution for the radiative photon energy k_{rad} shown in Fig. 2a: we observe a sharp peak for $k_{rad} < 0.04\ E_{beam}$ consistent within resolution with reaction (1) and a radiative tail, as expected from initial state radiation. Since radiative events can also be used for the exploration of new phenomena which could occur in reaction (1), we have kept in our sample events with $k_{rad} < .20\ E_{beam}$.

Since new physics such as μ^* production can be investigated in reaction (1) we have made a detailed study of the mass resolutions. From the known resolution of the angles of the photon and the charged particles, we expect a $\mu\gamma$ mass resolution, $\sigma_M^{angles} = 250\ \text{MeV} \cdot (E_{beam}/17\ \text{GeV})$ for a mass of 30.5 GeV (weakly dependent on the value of the mass). It is also possible to measure the same mass from the recoil momentum of the second muon with a small correction due to initial state radiation: such a determination competes in precision with the previous method only

for large $\mu\gamma$ masses, where the recoiling muon has a momentum not exceeding a few GeV/c. For example, a 30.5 GeV mass is reconstructed using the recoil muon momentum with a resolution $\sigma_M^{momentum} = 340$ MeV at $\sqrt{s} =$ 34 GeV rising to 2.4 GeV at $\sqrt{s} = 43$ GeV. We have two independent checks of our resolution: (i) the Monte Carlo simulation with known angular resolutions as input predicts correctly the energy resolution (1.3% of the beam energy) of the radiated photon along the beams as demonstrated in Fig. 2a, and (ii) there is good agreement between the two independent determinations of the $\mu\gamma$ mass - from angles or from momentum - where they have comparable precision (Fig. 2b). Therefore, we have used the combined determination with appropriate weights, yielding a mass resolution of 200 MeV (320 MeV) for a 30.5 GeV mass at $\sqrt{s} = 34$ GeV (43 GeV), respectively. We have also tried a complete 3C kinematic fit (allowing initial radiation along the beam direction) with no significant improvement in resolution; this is expected since the energy measurements of the fast muon and the photon bring little additional information at this level of precision. However, for those events where the computed radiative photon energy is consistent with zero, a 4C-fit has been attempted with an improvement in mass resolution of about a factor of 2. In summary, our analysis tells us that the events satisfy the kinematics of reaction (1) with the possible emission of an additional photon along the beam line and that a mass resolution of typically 200 MeV is achieved.

We have studied the possible contamination of the $\mu\mu\gamma$ sample from reactions (3) and (4) which involve missing energy: a maximum contribution of $2\ 10^{-2}$ of the $\mu\mu\gamma$ rate was estimated. However, in the domain defined by $M^2_{\mu\gamma}/s > .01$ and $M^2_{\mu\mu}/s > .01$, the contamination falls to a level of less than $6\ 10^{-3}$.

We have also examined the process where two photons are produced at large angles to the beam

$$e^+e^- \rightarrow \mu^+\mu^-\gamma\gamma \qquad (6)$$

They could simulate $\mu\mu\gamma$ events if one of the two photons escapes detection. If the energy of the second photon is larger than .5 GeV, we compute [5] a yield of 3.4 events at $\sqrt{s} > 33$ GeV, where we observe 3 events. Taking into account the detection losses and the kinematic fitting, we estimate the contamination to be less than $2\ 10^{-3}$ of the $\mu\mu\gamma$ rate.

In summary, for the region $M^2_{\mu\gamma}/s > .01$ and $M^2_{\mu\mu}/s > .01$ discussed below, the total contamination to the $\mu\mu\gamma$ sample is estimated to be less than $9\ 10^{-3}$ of the $\mu\mu\gamma$ rate expected from QED, decreasing to $3\ 10^{-3}$ for large $\mu\gamma$ masses.

Comparison with QED and Discussion

At the α^3 level a complete description of process (1) by QED is available[1] and widely used Monte Carlo generators exist. We have used such a program[4] and have also performed an independent Monte Carlo generation of events from reaction (1) which should be valid for hard radiation. We have included initial and final state radiative corrections to order α^4 following the prescription of Tsai[5]. We estimate our knowledge of the absolute normalization to be ± 10%.

All information concerning reaction (1) for unpolarised beams can be obtained from the Dalitz plot $(M^2_{\mu\mu}, (M^2_{\mu\gamma})_{low}, (M^2_{\mu\gamma})_{high})$, the orientation of the event plane with respect to the beam axis and the orientation of the event within this plane. We first consider the Dalitz plot population.

Since we are interested in possibly new phenomena, we apply cuts to avoid the regions where QED contributions are important, namely: $M^2_{\mu\mu}/s > .01$ and $M^2_{\mu\gamma}/s > .01$. These regions correspond to enhancements in the amplitudes for initial and final state radiation, respectively. Fig. 3 presents the experimental Dalitz plot distribution after these cuts. Since the data are spread over a large energy range, we use dimensionless variables scaled to the corresponding s values. Consequently, the Dalitz plot population should be energy-independent up to an overall normalisation factor. Figs. 3a and 3b show the Dalitz distributions for reaction (1) for $\sqrt{s} < 33$ GeV and $\sqrt{s} > 33$ GeV, respectively. To compare with QED, 3 regions are defined and their respective population is compared to the corresponding QED predictions in Table II. We observe good agreement with QED for all regions except in region III of Fig. 3b ($\sqrt{s} > 33$ GeV, $(M^2_{\mu\gamma})_{high}/s > .8$), where we observe 11 events and expect only 2.6. The probability that our observation in region III results from a statistical fluctuation of the expected QED rate is $9\ 10^{-5}$ (4 σ). To check that the effect is not generated by our experimental procedure, we have analyzed in a similar fashion our data for

reaction (2). The kinematics is identical within our cuts so that we are really testing our overall detection acceptance. The only expected difference comes from the additional t-channel amplitudes in the $ee\gamma$ process. Figs. 3c and 3d show the $ee\gamma$ Dalitz plots corresponding to the $\mu\mu\gamma$ cases discussed previously: here the agreement with the QED expectation[6] is good, in particular in region III for data above 33 GeV centre of mass energy (Table II).

The probability quoted above for a statistical fluctuaction of the QED distribution depends on the value chosen for the cut on $M^2_{\mu\gamma}/s$ used to define region III on the Dalitz plot. In order to assess the overall statistical significance of the observed effect independently of the position of this cut, we directly compared the experimental $\mu\gamma$ mass spectrum to the expected QED distribution. A Kolmogorov test gives a probability of compatibility of 310^{-3} for the data above $\sqrt{s} = 33$ GeV, for our standard cuts ($M^2_{\mu\gamma}/s$, $M^2_{\mu\mu}/s > .01$). When these cuts are not imposed, the probability even drops to 10^{-3}. Finally, we compared the experimental $\mu\gamma$ mass distributions below and above $\sqrt{s} = 33$ GeV: the probability that the two distributions are compatible is $2.5\ 10^{-2}$, which is obviously less significant due to the low statistics at lower energies, but it does not rely on the QED calculation.

To summarize, we observe an overall agreement with QED for both reactions (1) and (2) below $\sqrt{s} = 33$ GeV, but we have an excess of events for $\sqrt{s} = 33$ GeV for reaction (1) only, in a region where the effect of e-μ mass difference should be negligible. However the dominant t-channel exchange in the $ee\gamma$ reaction could mask any similar behaviour.

To proceed further in the understanding of this effect, we examine the mass distribution for large $\mu\gamma$ masses, since all events in region III of the Dalitz plot have masses larger than 30 GeV. In Fig. 4a the $\mu\gamma$ mass distribution for $\sqrt{s} > 33$ GeV shows an excess of events above QED in this region. Taking advantage of our good mass resolution in this range we have searched for structure in the mass distribution.

The result is given in Fig. 4b: all events are reasonably spread over the examined mass range, except for a cluster of 4 events centered at 30.6 ± 0.1 GeV with mass values which are consistent within experimental resolution. However the significance of this peak is only 2.2 σ when checked against the expected QED contribution in an 800 MeV bin (± 2σ). Even though we do not consider this peak to be significant, we have nevertheless examined the properties of these events, in view of a possible μ^* interpretation. However, the energy dependence (3 events at $\sqrt{s}$ = 34 GeV and 1 at 43 GeV) and the distribution of the photon angle with respect to the beam line are inconsistent with this interpretation, at least in a simple approach[7].

Fig. 4c shows the μμ-mass distribution for $\sqrt{s}$ > 33 GeV. Again no significant narrow structure is observed.

We have examined other variables besides the invariant masses. Instead of the angular distribution of the normal to the μμγ plane with respect to the beam direction, we have chosen the distribution of the photon angle: no marked deviation from the QED expectation is observed as shown in Fig. 5. In particular, the events in the abnormally populated corner of the Dalitz plot are as peaked as the initial state radiation with its characteristic $(1 + \cos^2\theta)/\sin^2\theta$ behaviour in this region (shaded area in Fig. 5).

We have not yet found any satisfactory explanation for the events exceeding the QED rate. No strong energy dependence is observed: the 11 events split as 7:4 between $\sqrt{s}$ = 34 and 43 GeV, where the corresponding expected rates from QED are 1.4 : 1.2.

Previous analyses of reaction (1) have been reported. The data from MAC[8] at $\sqrt{s}$ = 29 GeV are in good agreement with QED, like our data in the lower energy range. The analysis performed by MARK J[9] on data taken at $\sqrt{s}$ up to 36.7 GeV indicates no deviation from QED but the sensitivity is reduced at large μγ masses (no cuts on $M_{\mu\mu}$ and $M_{\mu\gamma}$ are applied against QED): no results are given above a mass of 30.5 GeV and the mass resolution is quoted to be ∿1 GeV. JADE has recently published[10] an analysis of reaction (1) using again data at $\sqrt{s}$ up to 36.7 GeV with a mass resolution of ∿1 GeV: no excess above QED is observed for $M_{\mu\gamma}$ > 30 GeV. Although the low value chosen for the cut $M_{\mu\mu}$ > 1.2 GeV reduces the sensitivity to an extra contribution, the data as they are presented seem to be in disagreement with our findings.

In conclusion, we have observed an excess of events over the expected QED rate in the reaction $e^+e^- \to \mu^+\mu^-\gamma$ in the high μγ mass region of the Dalitz plot. The excess appears for $\sqrt{s}$ > 33 GeV and $(M^2_{\mu\gamma})_{high}/s$ > 0.8. The probability that the effect is due to a statistical fluctuation is at the 10^{-3} level.

Acknowledgement

We gratefully acknowledge the outstanding efforts of the PETRA machine group which enabled these measurements. We are indebted to the DESY computer center for their excellent support during the experiment. We acknowledge the invaluable effort of all engineers and technicians of the collaborating institutions in the construction and maintenance of the apparatus, in particular the operation of the magnet system by M. Clausen and the cryogenics group. The visiting groups wish to thank the DESY directorate for the support and kind hospitality extended to them. This work was partly supported by the Bundesministerium für Forschung und Technologie (Germany), by the Commissariat à l'Energie Atomique and the Institut National de Physique Nucléaire et de Physique des Particules (France), by the Science and Engineering Research Council (UK), and by the Israeli Ministry of Science and Development.

REFERENCES

(1) F. Berends, K. Gaemers, R. Gastmans
Nucl.Phys. B57 (1973), 381; Nucl.Phys. B63 (1973), 381
F. Berends, R. Kleiss, Nucl.Phys. B177 (1981), 237
F. Berends, R. Kleiss, S. Jadach, Nucl.Phys. B202 (1982), 63

(2) H.-J. Behrend et al., CELLO Coll., Physica Scripta 23 (1981), 610

(3) H.-J. Behrend et al., CELLO Coll., Phys.Lett. 114B (1982), 282
H.-J. Behrend et al., CELLO Coll., Phys.Lett. 127B (1983), 270

(4) The Monte Carlo generator was based on the paper of F. Berends, R. Kleiss and S. Jadach, quoted in (1)

(5) Y.S. Tsai, SLAC-Pub 3129 (1983)

(6) F. Berends, K. Gaemers, R. Gastmans
Nucl.Phys. B68 (1974), 541
F. Berends, R. Kleiss, Nucl.Phys. B228 (1983), 537

(7) A.M. Litke, PhD Thesis, Harvard University (1970)
H. Terazawa et al., Phys.Lett. 112B (1982), 387

(8) W.T. Ford et al., MAC Coll., Phys.Rev.Lett. 51 (1983), 257

(9) B. Adeva et al., MARK J Coll., Phys.Rev.Lett. 48 (1982), 967

(10) W. Bartel et al., JADE Coll., DESY 84-033 (1984)

Table I: Data sample for the process $e^+e^- \to \mu^+\mu^-\gamma$ within the cuts described in the text

CM Energy (GeV)	Integrated Luminosity (pb^{-1})	Number of Events
14	.6	8
22	1.7	14
34-36.7	10.1	21
40-46.8	11.4	20
		63

Table II: Population of the Dalitz plot in 3 regions

reaction	$\sqrt{s}$ (GeV)		Region I	Region II	Region III
$ee \to \mu\mu\gamma$	14 - 22	data	8	9	0
		MC	7.0	7.4	1.4
	33 - 46	data	10	10	11
		MC	13.6	14.1	2.6
$ee \to ee\gamma$	14 - 22	data	80	76	17
		MC	90.1	71.4	9.7
	33 - 46	data	158	130	16
		MC	158.2	124.0	16.0

region I $.6 < M^2_{\mu\mu}/s < .9$

region II $M^2_{\mu\mu}/s < .6$ and $M^2_{\mu\gamma}/s < .8$

region III $M^2_{\mu\gamma}/s > .8$

in addition $M^2_{\mu\gamma}/s > .01$ and $M^2_{\mu\mu}/s > .01$

FIGURE CAPTIONS

Fig. 1a: The transverse energy deposition of the tracks in the lead liquid argon calorimeter

Fig. 1b: The ratio (Q) of the distance between the extrapolated impact of a track in the muon chamber and the recorded hit (d) to the estimated position uncertainty (σ)

Fig. 2a: The distribution of $x_{rad} = k_{rad}/E_{beam}$ for the computed radiative photon along the beam line

Fig. 2b: The difference between the $\mu\gamma$ invariant mass calculated from the angle measurements of the particle tracks and the invariant mass computed from the momentum measurement of the slow μ ($p_\mu < 4$ GeV).

Fig. 3a,b,c,d: The Dalitz-plot population for the reaction $ee \to \mu\mu\gamma$ and $ee \to ee\gamma$ for the two different energy regions

Fig. 4a: The distribution of the muon-photon invariant masses (2 entries per event). The curve is the prediction from the QED Monte Carlo calculation

Fig. 4b: The distribution of the muon-photon invariant masses with their estimated uncertainties (25-45 GeV)

Fig. 4c: The distribution of the muon-muon invariant mass. The curve is the prediction from the QED Monte Carlo calculation

Fig. 5: The distribution of the cosθ of the photon with respect to the e^- beam direction

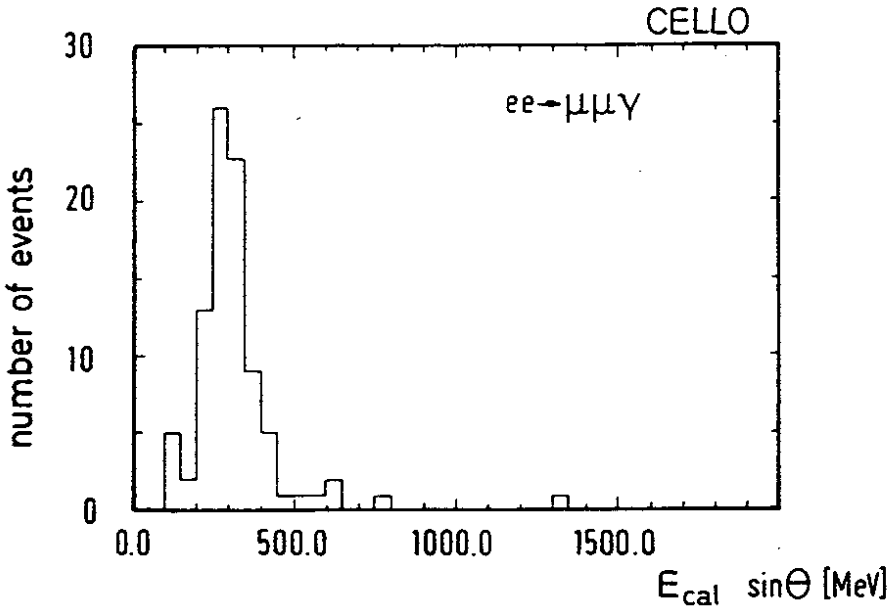

Fig. 1a

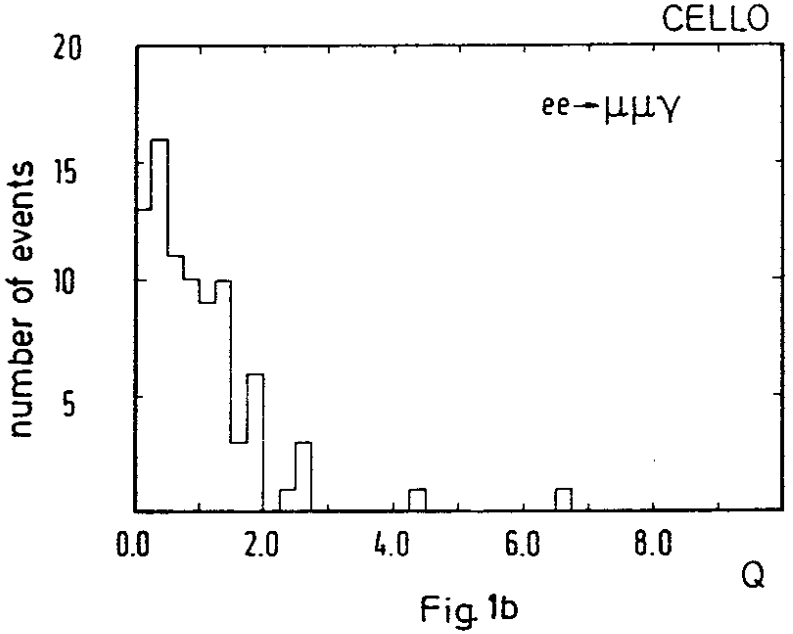

Fig. 1b

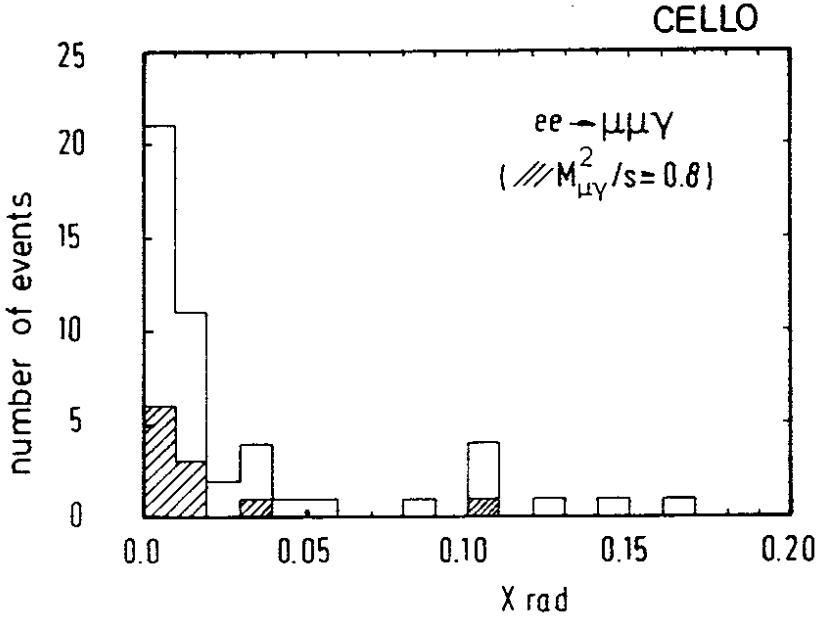

Fig. 2a

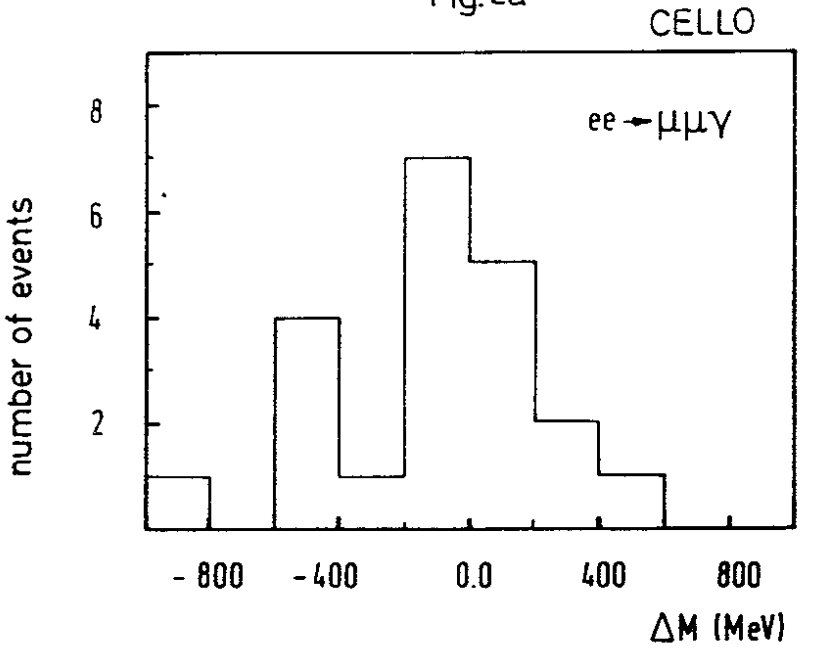

Fig. 2b

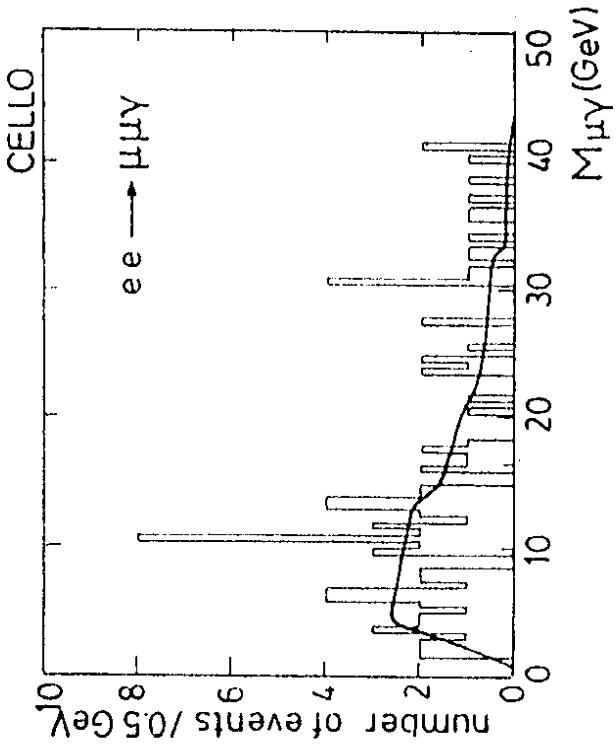
CELLO
e e → μμγ
number of events /0.5 GeV
$M_{\mu\gamma}$(GeV)

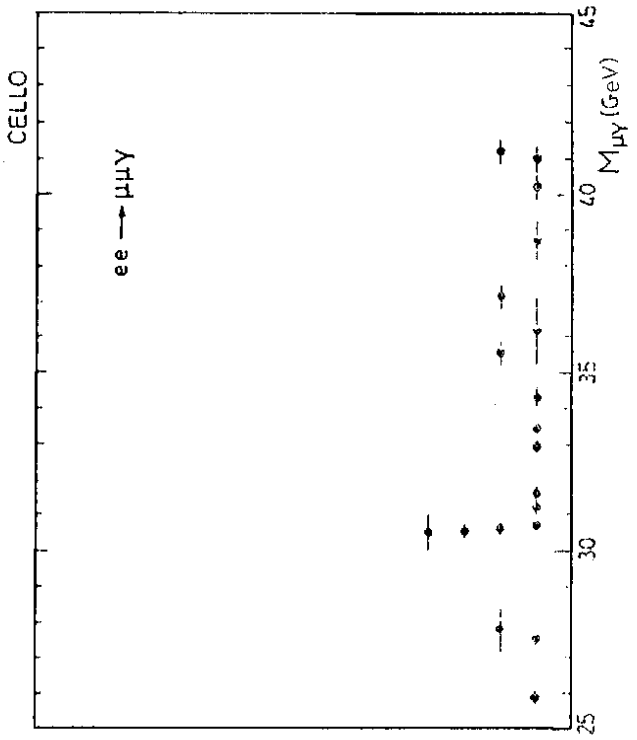
CELLO
e e → μμγ
$M_{\mu\gamma}$(GeV)

Fig. 4b

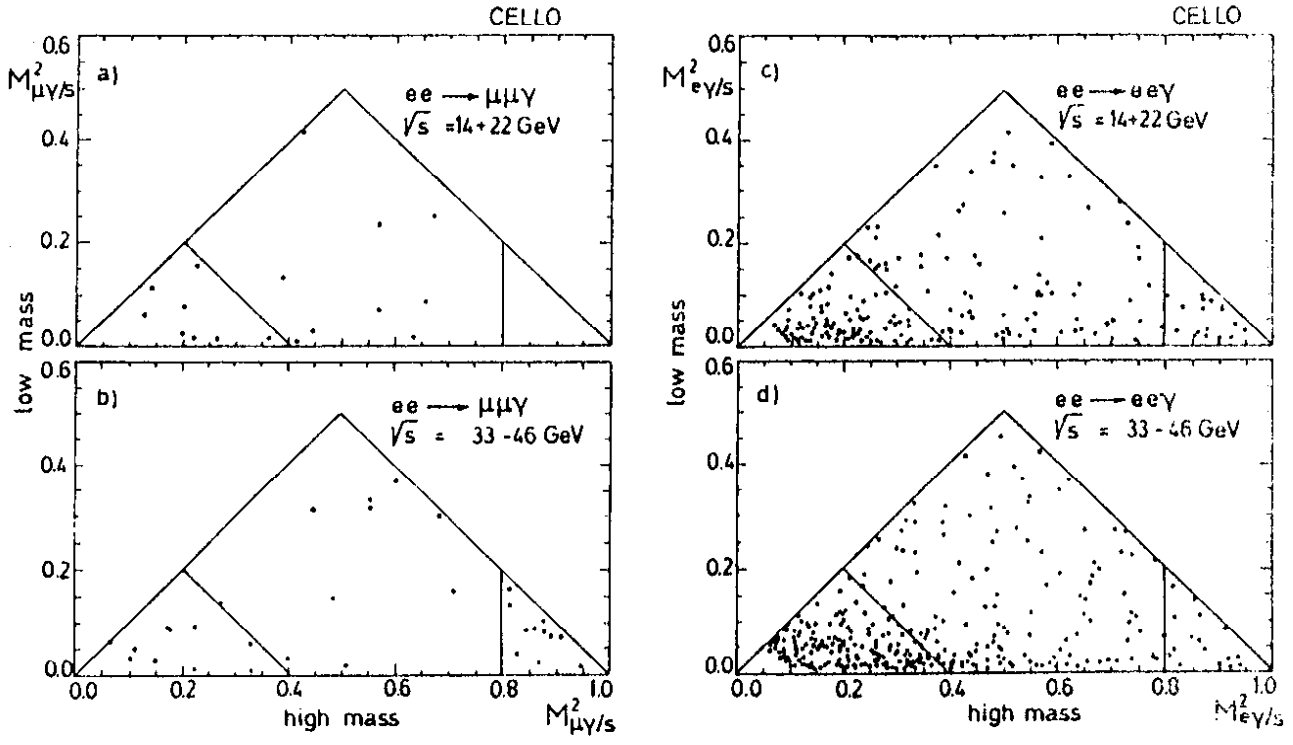
CELLO
a)
e e → μμγ
√s =14+22 GeV
b)
e e → μμγ
√s = 33 -46 GeV
low mass
high mass
$M^2_{\mu\gamma/s}$
c)
e e → e eγ
√s = 14+22 GeV
d)
e e → e eγ
√s = 33 - 46 GeV
$M^2_{e\gamma/s}$

Fig. 3

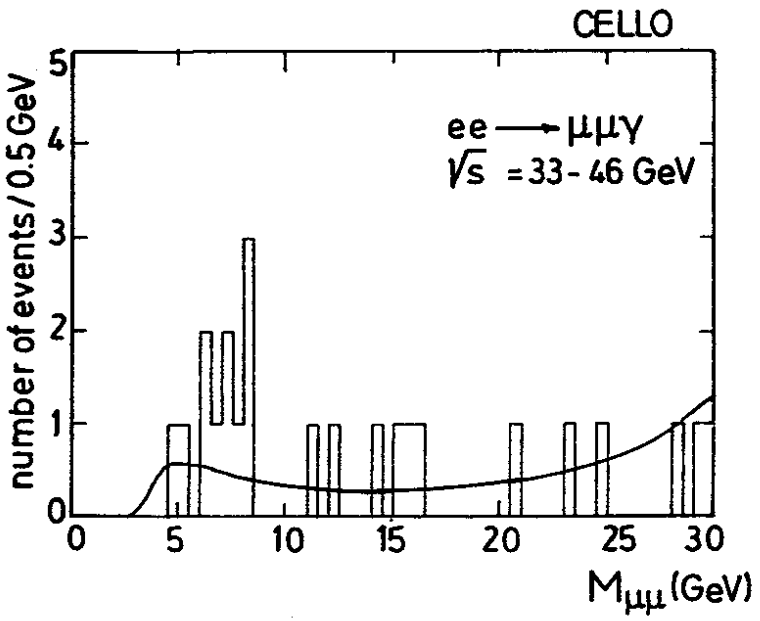
CELLO
ee → μμγ
√s = 33 - 46 GeV
number of events / 0.5 GeV
0
1
2
3
4
5
0
5
10
15
20
25
30
Mμμ (GeV)

Fig. 4c

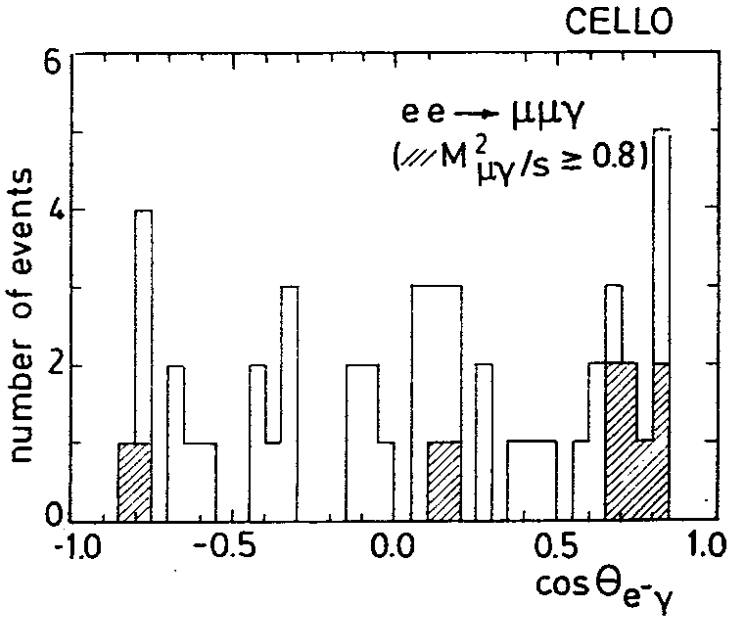
CELLO
e e → μμγ
(/// M²μγ /s ≥ 0.8)
number of events
0
2
4
6
-1.0
-0.5
0.0
0.5
1.0
cos Θe⁻γ

Fig. 5